Outward expansion of the lunar wake: ARTEMIS observations

H. Zhang,[1,2] K. K. Khurana,[3] Q.-G. Zong,[4] M. G. Kivelson,[3,5] T.-S. Hsu,[3] W. X. Wan,[1] Z. Y. Pu,[4] V. Angelopoulos,[3] X. Cao,[1] Y. F. Wang,[4] Q. Q. Shi,[6] W. L. Liu,[7] A. M. Tian,[6] and C. L. Tang[6]

Received 21 June 2012; revised 5 August 2012; accepted 6 August 2012; published 21 September 2012.

[1] Magnetohydrodynamics (MHD) predicts that lunar wake expands outward at magnetosonic velocities in all directions perpendicular to background solar wind; however, fluid theories emphasize that lunar wake expands outward at sound speeds mainly along the interplanetary magnetic field (IMF). Early observations supported the MHD predictions in the near-moon region despite lack of solar wind and IMF observations. Thanks to the special orbit design of the ARTEMIS mission, the solar wind conditions are well determined at the time of concurrent observations in the lunar wake. 164 wake crossings made by ARTEMIS are statistically studied in this paper. Observations indicated that, in either distant or near-Moon regions, the lunar wake expands outward at the fast MHD wave velocities. This simple model provides a powerful way to determine wake boundaries, particularly at large distances where the boundary signatures are indistinct, thus allowing further studies on the Moon-solar wind/crustal field-solar wind interactions. **Citation:** Zhang, H., et al. (2012), Outward expansion of the lunar wake: ARTEMIS observations, *Geophys. Res. Lett.*, *39*, L18104, doi:10.1029/2012GL052839.

1. Introduction

[2] Earth's Moon is generally considered as a non-conductive body without a global-scale magnetic field and atmosphere, therefore lacking a global magnetosphere and an ionosphere, although some small scale crustal magnetic anomalies exist on its surface. When immersed within and interacting with the supersonic solar wind, the Moon acts as an absorber for the solar wind plasma, and a plasma void forms behind [*Colburn et al.*, 1967; *Ness et al.*, 1967]. The interplanetary magnetic field (IMF), however, passes through this insulator basically undisturbed [*Sonett*, 1982]. A complicated plasma and field structure forms behind the Moon when plasma refills, which is referred to as the 'lunar wake'. Simulations have predicted that the lunar wake may extend many lunar radii downstream of the Moon [e.g., *Holmstrom et al.*, 2012]. The most distant wake crossing occurred at $\sim$25 R_M (lunar radius) downstream when the Wind spacecraft skimmed over the Moon [*Clack et al.*, 2004].

[3] Even though kinetic effects contribute to the refilling of the wake [e.g., *Halekas et al.*, 2011, and references therein], MHD theory provides a good enough way to understand many features of the plasma entry and the subsequent large-scale structure of the lunar wake. When the plasma void forms behind the Moon, the ambient solar wind and magnetic field expand into the void due to pressure depletion. The field in the void is thus compressed, resulting in field magnitude enhancement; however, near but outside the void boundary, the expansion leads to depletion of the plasma density and the field magnitude and a rarefaction front propagates away into the nearby solar wind. This plasma and field depletion region is referred to as an 'expansion region' which surrounds the field-enhanced central wake [e.g., *Whang*, 1968; *Johnson and Midgley*, 1968; *Michel*, 1968].

[4] The outward propagation of rarefaction front, which is referred to as the wake boundary (WB) in this paper, has been extensively studied since the Explorer and Apollo Missions in 1960s. By means of MHD approach, *Johnson and Midgley* [1968] and *Michel* [1968] predicted that the wake expands outward at fast magnetosonic velocities. Fluid theories, however, predict that the outer boundary expands only in the field-aligned directions at ion acoustic speeds $(\gamma P/\rho)^{1/2}$, where γ is the adiabatic coefficient, P is pressure and ρ is the mass density [*Denavit*, 1979; *Samir et al.*, 1983; *Farrell et al.*, 1998; *Clack et al.*, 2004]. To examine these theoretical predictions, simulations provide a powerful way to view the global picture of the lunar wake. It is clearly shown, for example, in a 3D hybrid simulation that the rarefaction front moves away at fast magnetosonic velocities in the rest frame of solar wind [*Wiehle et al.*, 2011; *Holmstrom et al.*, 2012; *Wang et al.*, 2011]. In-situ satellite observations confirmed the MHD prediction in the near-Moon downstream region (within 2 R_M) [*Whang and Ness*, 1970]. As for the more distant downstream region, so far only one event was reported that the WB location satisfied the MHD prediction at $\sim$6 R_M [*Owen et al.*, 1996]. Recently, the field-aligned particle refilling process was emphasized by the Wind observations in the distant downstream region (>6 R_M), which, however, could be readily interpreted within the fluid theory frame [*Ogilvie et al.*, 1996]. Certainly more observations are needed, especially at large downstream distances.

[1]Beijing National Observatory of Space Environment, Institute of Geology and Geophysics, Chinese Academy of Sciences, Beijing, China.
[2]State Key Laboratory of Space Weather, Chinese Academy of Sciences, Beijing, China.
[3]Department of Earth and Space Sciences, University of California, Los Angeles, California, USA.
[4]School of Earth and Space Sciences, Peking University, Beijing, China.
[5]Atmospheric, Oceanic and Space Sciences Department, University of Michigan, Ann Arbot, Michigan, USA.
[6]School of Space Science and Physics, Shandong University at Weihai, Weihai, China.
[7]School of Astronautics, Beihang University, Beijing, China.

Corresponding author: H. Zhang, Beijing National Observatory of Space Environment, Institute of Geology and Geophysics, Chinese Academy of Sciences, Beijing 100029, China. (hzhang@mail.iggcas.ac.cn)

0094-8276/12/2012GL052839

[5] Except for the limited data coverage, the other uncertainty derives from lack of precisely-determined solar wind and IMF conditions associated with WB crossings [*Whang and Ness*, 1970; *Ogilvie et al.*, 1996]. Except that the wake expansion velocity depends on the solar wind and IMF conditions, the plasma refilling may also depend on the angle between the solar wind and IMF [e.g., *Holmstrom et al.*, 2012].

[6] In this study, however, thanks to the special orbit design of the two spacecraft ARTEMIS mission [*Angelopoulos*, 2011], the rarefaction front can be studied with well-determined solar wind and IMF conditions and large data coverage. When one ARTEMIS spacecraft crosses the lunar wake, by design, the other one is located within the nearby solar wind, implying that the solar wind and IMF conditions can be precisely obtained [*Sibeck et al.*, 2011]. From June of 2011 to February of 2012, the ARTEMIS spacecraft have made 164 wake crossings at various distances from 100 km to 19,000 km (0.06∼11 R_M). In the next section, we present a case study and statistical studies; in Section 3 our observations are briefly discussed and summarized.

2. ARTEMIS Observations

2.1. Instrumentation and Coordinate System

[7] The ARTEMIS mission, an extension of the THEMIS mission, consists of two spacecraft, P1 and P2. Since July 26, 2011, both spacecraft were trapped in equatorial and high-eccentricity lunar orbits with perigee and apogee of ∼100 km (0.6 R_M) and 19,000 km (11 R_M), respectively [*Angelopoulos*, 2011]. The orbits are designed to have one spacecraft remaining in the solar wind near the Moon when the other one traverses the lunar wake, such that it provides a unique opportunity to explore the lunar wake at various distances with unambiguously known solar wind and interplanetary magnetic field (IMF) conditions. All data analyzed in the present study were collected by the electrostatic analyzer (ESA) [*McFadden et al.*, 2008] and the fluxgate magnetometer [*Auster et al.*, 2008], and they are used at a 3 second resolution.

[8] To exclude the effects of IMF clock angles and solar wind directions, a dynamic orthogonal coordinate system is introduced in this study, which is referred to as 'Lunar Solar Magnetic' system (LSM). In this system, X always points against the instantaneous solar wind, which is dynamic and changes its direction and magnitude all the time; Y is along the direction of cross product of instantaneous IMF and X; Z completes the orthogonal set through X × Y; the center of the Moon is set to be the origin of the system. In this dynamic coordinate system, the velocity of the background solar wind is always along −X, and the IMF is always contained within the X − Z plane (perpendicular to Y). Hereafter in this paper, the region with $(Y^2 + Z^2)^{1/2} < 1$ R_M and $X < 0$ R_M is referred to as the 'solar wind shadow' region, which is distinct from the 'sunlight shadow' region since the velocity of solar wind is not necessarily along the direction radially away from the sun.

2.2. A Lunar Wake Crossing Event on December 19th, 2011

[9] A wake crossing event on December 19th, 2011 is presented here. From 15:00 UT to 18:00 UT, the Moon was located around [21.3, −53.4, −4.4] R_E in the Geocentric Solar Ecliptic (GSE) coordinate system. Spacecraft P2 remained in the solar wind at about 9 R_M downstream from the Moon (not shown) and monitored the background solar wind and IMF conditions. Figure 1a shows the trajectory of spacecraft P1 in the LSM coordinate system. P1 moved inbound from X = −3.5 R_M, and entered into the solar wind shadow at about X = −2.8 R_M (marked as SB1). At X = −1.2 R_M P1 left the solar wind shadow (marked as SB2) and subsequently reached the dayside of the Moon (X > 0). Figure 1b1 shows the location of P1 as function of time; the blue line represents X and the green line denotes the distance of spacecraft from the X axis ($(Y^2 + Z^2)^{1/2}$). The black bar at the top indicates the 'sunlight shadow' region, and the blue bar at the bottom shows the 'solar wind shadow' region.

[10] Figures 1b2–1b7 present plasma and magnetic field data of this event. Data from P2, which remained in the solar wind, are plotted in black; data from P1, which crossed the wake, are plotted in red. We identify the point where the ion number density begins to decrease relative to the density of the undisturbed solar wind as the 'wake boundary' (WB). As shown in Figure 1b2, before 15:52 UT, the ion number density (Ni) measured at the two spacecraft tracks each other closely, although there is a very small offset between them. At 15:52 UT Ni at P1 began to decrease but Ni at P2 remained at the previous level. This is the first WB encountered in this event (the first red vertical dashed line, marked as 'WB1'). Ni decreased slowly in the wake until P1 reached the solar wind shadow boundary at about 16:12 UT (the first black vertical dashed line, marked as 'SB1'). Once P1 entered into the solar wind shadow, Ni dropped much more quickly than before to a level below 0.1 cm^{-3}. P1 remained in the solar wind shadow for about 50 minutes and left at 17:00 UT (the second black vertical dashed line, marked as 'SB2'). Then, Ni recovered slowly to the background level until P1 reached the WB again at 17:12 UT (the second red vertical dashed line, marked as 'WB2'). Thereafter, P1 returned to the undisturbed solar wind and Ni recovered to the background solar wind level.

[11] Our data indicate that the WB expands away from the lunar terminator in the rest frame of the solar wind as the downstream distance increases. As shown in Figure 1a, at X ∼ −0.8 R_M ('WB2'), the WB was located ∼0.2 R_M away from the solar wind shadow; at X ∼ −3.1 R_M ('WB1'), however, the boundary was 0.76 R_M away from the solar wind shadow. We can estimate the WB expansion velocity. The first boundary was encountered by P1 at [−3.08, 0.61, 1.65] R_M in the LSM system, and it took about $T1 = d1/V_{SM}$ = 15.88 seconds for the undisturbed solar wind (V_{SW} = −343.9 km/s) to move from the Moon to the location of the spacecraft (d1 = 3.08 R_M). Let us assume that the density perturbations are excited at the terminator of the Moon and they propagate radially away in Y − Z plane in the rest frame of solar wind. Within this 15.58 seconds, this density perturbation front propagated d2 = 0.76 R_M radially in the Y − Z plane and reached the location of P1, which gives a propagation velocity of d2/T1∼85 km/s. We notice that when the perturbation propagates away from the lunar terminator, it reduces the field magnitude (Figure 1b3 between WB1 and SB1) and the magnetic pressure (Figure 1b4). Although only higher energy particles (high temperatures) present in the central wake (Figures 1b6 and 1b7), the significant drop of the ion number density (Figure 1b2) leads to a

depletion of thermal pressure inside the wake (Figures 1b5). The in-phase changes in the magnetic and the thermal pressure suggest that the perturbation front propagates at fast wave velocities. We calculated the corresponding fast mode wave velocities through $V_F = [(C_S^2 + V_A^2 + ((C_S^2 + V_A^2)^2 - 4C_S^2V_A^2 \cos^2\theta)^{1/2})/2]^{1/2}$, where Cs denotes the background solar wind sound speed, V_A is the solar wind Alfvén velocity, and θ is the angle between the wave vector and the IMF. For the first WB (WB1), Cs = 63 km/s, V_A = 55 km/s, and θ = 65 degrees (Here, we assume that the perturbation propagates radially out in the Y − Z plane from the lunar terminator in the rest frame of the solar wind), all of which give the fast mode velocity of 79 km/s, which is approximately equal to our calculated velocity, 85 km/s. In the same way, the propagation velocity for the second boundary 'WB2' was calculated to be 95 km/s, which is also close to the corresponding fast mode velocity, 97 km/s.

[12] The fast mode wave may not propagate purely radially from the lunar terminator in the Y − Z plane; here we present another way to demonstrate that the WB propagates at the fast wave velocity. In Figure 1b8, the blue curve gives the time taken by solar wind to propagate from the Moon to the location of the spacecraft P1 (T1 = d1/V_{SW}), where d1 is the distance of P1 to the Moon in the X direction and V_{SW} is the instantaneous solar wind velocity; the green curve represents the shortest time, T2, required for the fast waves to propagate from anywhere on the lunar surface of to the location of P1 (it is not exactly d2/V_F) in the rest frame of solar wind. When T1 < T2, it means that when the solar wind reaches P1, the fast wave perturbations have not yet propagated to the location of P1 (a fast wave requires more time than does the solar wind); T1 > T2 means that when the solar wind arrives at P1, the fast wave has already passed by P1 (a fast wave needs less time to reach P1 than does the solar wind). In our data, however, at the WBs identified by the ion number density (the red vertical dashed lines in Figure 1b), T1 is roughly equal to T2, which means that when the solar wind reached P1, the fast wave also arrived at P1. This result strongly suggests that the WB propagates at fast wave velocities in the rest frame of the solar wind.

2.3. Statistical Studies

[13] From June 27th, 2011 to February 3rd, 2012, there were 164 wake crossing events, e.g., at least 328 (164 × 2) boundary crossings. As the case study, we identified the WBs by using decrease in ion number density. Plasma and magnetic field data are available for both P1 and P2 for only 264 of the boundary crossings, thus only these events are involved in this statistical study. In the same way as in our case study, we then calculated the corresponding times, T1 = d1/V_{SW} and T2, at these boundaries (Figure 2a). The scatter plot of T1 and T2 for the 264 boundary crossings is shown in Figure 2b. Data points scatter around the diagonal of the plot. A linear regression gives T2 = 0.95T1 + 0.68 as shown

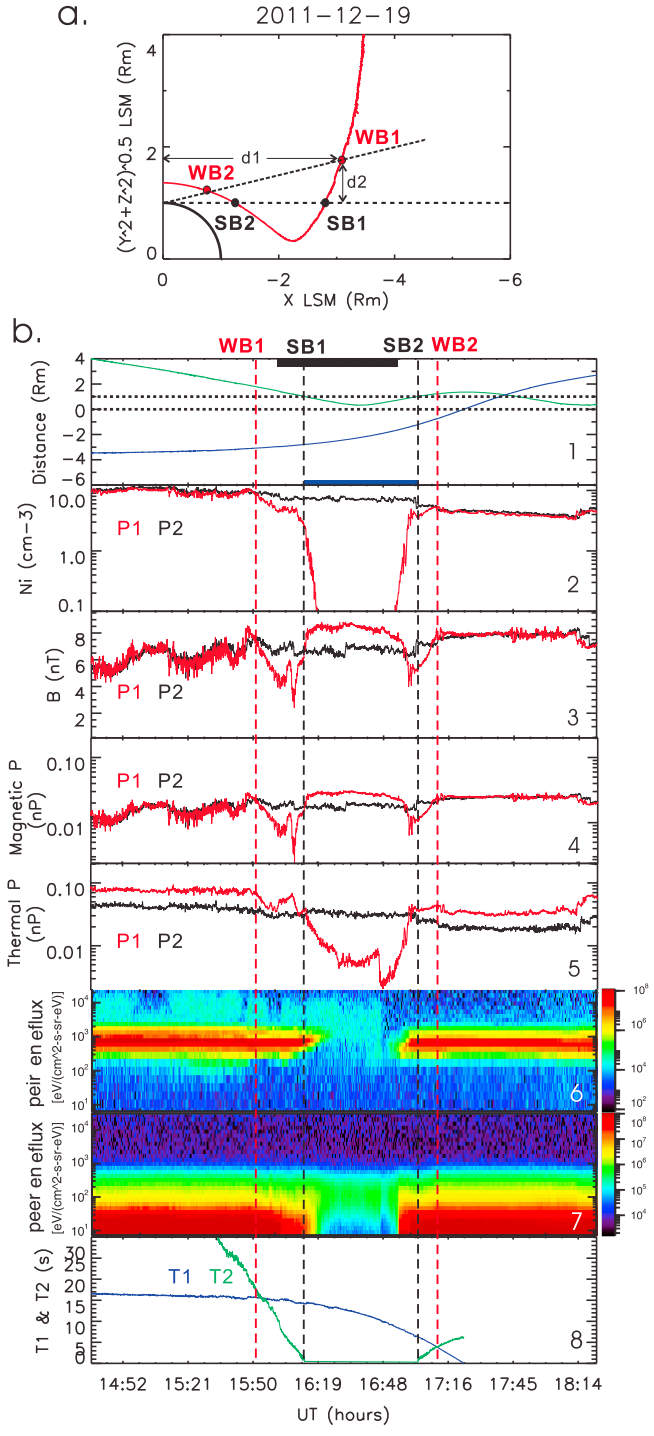

Figure 1. A lunar wake crossing event on December 19th, 2011. (a) shows the distance of spacecraft P1 to the X axis of the LSM coordinate system $(Y^2 + Z^2)^{1/2}$ as function of X. WB1 and WB2 denote locations of two wake boundary crossings, and SB1 and SB2 denote two solar wind shadow boundary crossings. (b1) These two position parameters, $(Y^2 + Z^2)^{1/2}$(green) and X (blue) for P1 are also shown as functions of time. (b2–b7) The ion number densities, the field magnitudes, the magnetic pressures, the thermal pressures, and the ion and electron energy spectra (P1) are plotted. The black curves for spacecraft P2, which remained in the nearby solar wind; and the red for P1, which crossed the wake. (b8) The time (T1) needed for the solar wind to propagate from the Moon to the location of P1 is shown in blue, and the shortest time (T2) taken by fast mode waves excited anywhere on the lunar surface to propagate to the location of P1 in the rest frame of the solar wind is shown in green.

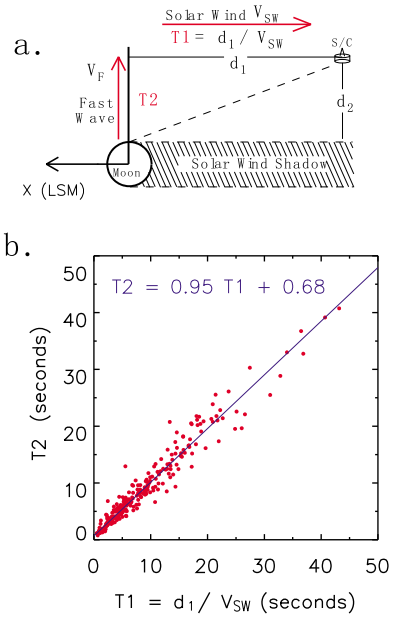

Figure 2. (a) The sketch of the outward expansion of lunar wake is shown. *d*1 denotes the distance of the wake crossing spacecraft to the Moon in the X direction, V_{SW} is the instantaneous solar wind velocity, *d*2 is the distance of spacecraft to the solar wind shadow boundary, V_F stands for the velocity of the fast wave excited on the lunar surface, and T1 and T2 are the same as described in Figure 1 but calculated on the WBs. (b) A scatter plot of T1 and T2 for 264 WBs are plotted. A linear regression of T2 to T1, given by T2 = 0.95T1 + 0.68, is shown by the blue line.

by the blue line in Figure 2b. T2 is roughly equal to T1, which is consistent with the MHD assertion that the WBs propagate outward at fast wave velocities.

[14] The outward expansion of the lunar wake is demonstrated more intuitively in Figure 3. All available ion number density data for 164 wake crossing events, $N_{i,wake}$, are normalized by the background solar wind number density ($N_{i,wake}/N_{i,solarwind}$) and shown the LSM coordinate system. To exclude the effect of the dynamic solar wind velocities, the locations of the data points in the X direction are normalized by the instantaneous solar wind velocities V_{SW} (X/V_{SW}). The lunar wake is then divided into three different regions, Region I (X/V_{SW} = [0, 15] seconds), Region II (X/V_{SW} = [15, 30] seconds) and Region III (X/V_{SW} > 30 seconds) as shown in Figure 3a. Figure 3b1 shows the distribution for Region I in the Y − Z plane of the median values of the normalized number densities $N_{i,wake}/N_{i,solarwind}$ within bins with $dY = 0.1\ R_M$ and $dZ = 0.1\ R_M$. The solid black circle shows the solar wind shadow boundary projected in the Y − Z plane, and the solid ellipse is the fast wave front calculated by using the median values of the solar wind sound speeds Cs, Alfvén velocities V_A, IMF directions, and the solar wind propagation times in Region I. Outside the calculated fast wave front, the color is dominantly pink or red ($N_{i,wake}/N_{i,solarwind} \sim 1$), denoting the undisturbed background level solar wind. The lunar wake, represented by the decrease in the ion density ($N_{i,wake}/N_{i,solarwind} < 1$), is found to be confined well within the calculated fast wave front. Just inside the fast wave front, the color is dominantly blue ($N_{i,wake}/N_{i,solarwind}$ 0.7∼0.9), and the refilling process begins to reduce plasma densities. While inside the solar wind shadow, the density drops rapidly from 0.7 (dominantly blue and green) to a level below 0.1 (black). Figure 3b2 shows profiles of $N_{i,wake}/N_{i,solarwind}$ along the Y axis (blue) and along Z axis (red) in Figure 3b1. It is clear that $N_{i,wake}/N_{i,solarwind}$ begins to reduce at the fast wave fronts denoted by the two blue and two red vertical lines (blue for the fast wave fronts in the Y direction, red for the fronts in the Z direction). The formats of Figures 3c1, 3c2, 3d1, and 3d2 are analogous to those of Figures 3b1 and 3b2, whereas the data points are limited within Regions II and III, respectively. It is found: (1) the WBs move away from the lunar terminator as the downstream distance increases; (2) WBs are always located near the fast wave front. These observations reveal that the lunar wake expands outward at fast wave velocities. Certainly, the location of WBs may also be adjusted by angles between the solar wind velocities and the IMF; however, in Figure 3, we do not have enough data to distinguish the effect of these angles.

3. Discussion and Summaries

[15] To prove that the wake is formed by fast wave, we use evidence from more plasma and magnetic field observations. Figure 4 plots the normalized ion temperatures ($T_{i,wake}/T_{i,back}$), electron temperature ($T_{e,wake}/T_{e,back}$), thermal pressure (sum of ion and electron pressures) and field magnitude ($B_{T,wake}/B_{T,Solarwind}$). All formats are the same as those in Figure 3. Although the ion and electron temperatures enhance significantly in the central wake (Figures 4a and 4b) due to the earlier arrival of the hot ions and electrons with higher thermal velocities (Figures 1b6 and 1b7), the total thermal pressure decreases in the lunar wake (Figure 4c, Regions I and II), particularly in the near-Moon region, mainly because of the depletion of plasma. An outward thermal pressure gradient thus forms on the wake boundary. The field magnitudes increase up to 1.2 in the central wake of the near-Moon region (Region I) and to higher levels further downstream (Region II and III); whereas in the region outside of the solar wind shadow but inside the fast wave front, the normalized field magnitudes drop to levels below 1.0. This field magnitude pattern can be easily understood by a diamagnetic current system resulting from thermal pressure gradient on the WB [*Colburn et al.*, 1967; *Ness et al.*, 1967]. The in-phase changes in magnetic pressure and thermal pressure is consistent with the properties of the fast mode. This analysis further confirms that, to a first order, the lunar wake itself can be treated as a fast wave front excited at the terminator of the Moon through the absorption of solar wind plasma [*Holmstrom et al.*, 2012].

[16] Solar wind plasma absorption is not the only fast wave source, and the interaction between solar wind and the magnetic anomalies on the lunar surface may also excite fast waves. Solar wind interaction with small scale field anomalies may vary as the magnitudes of these anomalies increase [*Omidi et al.*, 2002]. For the lunar anomaly case, the interaction should be magnetosonic and it yields compression of the field magnitude, which propagates outward around the wake. The field compression is common to see around the lunar wake [e.g., *Halekas et al.*, 2006]. Field

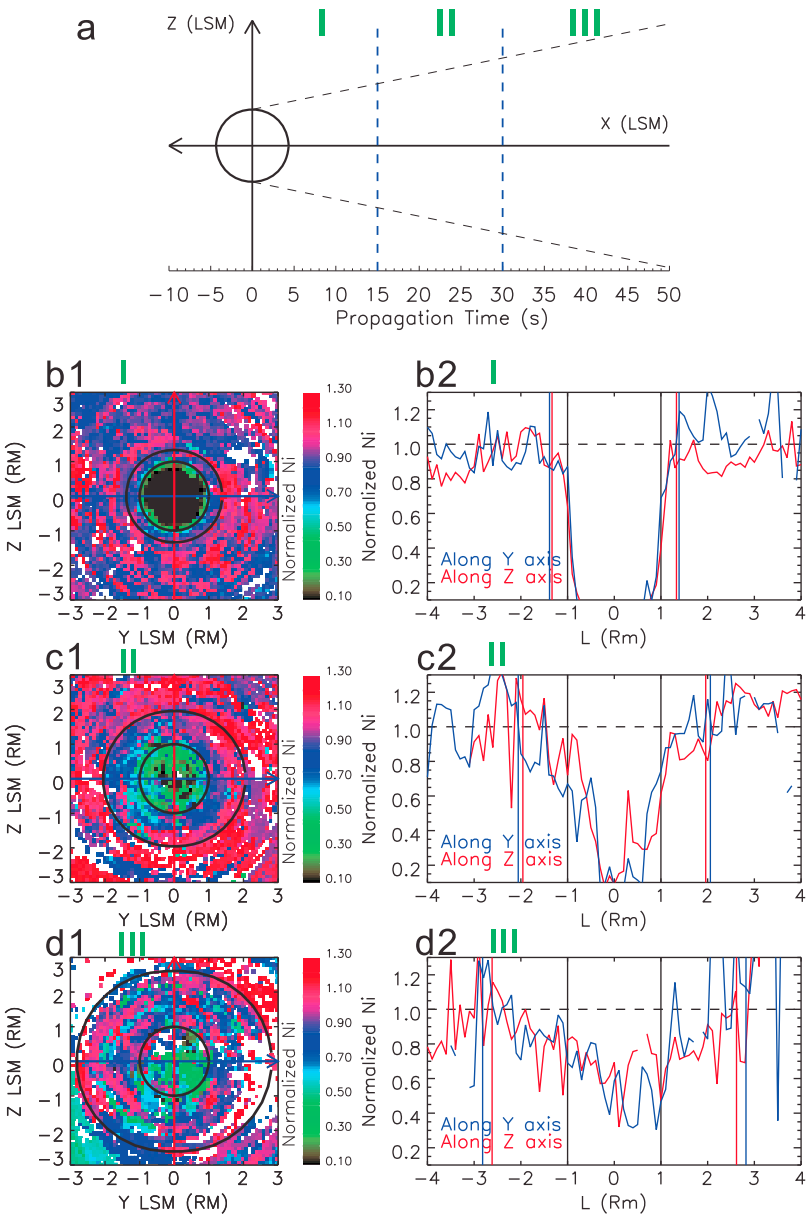

Figure 3. The distribution of the normalized ion number density ($N_{i,wake}/N_{i,solarwind}$) inside and around the lunar wake. (a) Three downstream regions with $X/V_{SM} < 15$ (Region I), $15 < X/V_{SM} < 30$ (Region II), and $X/V_{SM} > 30$ seconds (Region III), respectively. (b1) The distribution of the median values of the normalized ion number densities ($N_{i,wake}/N_{i,solarwind}$) within bins with $dY = 0.1\ R_M$ and $dZ = 0.1R_M$ for measurement within region 'I'. The central black circle is the projection of the solar wind shadow boundary on the Y − Z plane, and the black ellipse is the calculated fast mode front. (b2) The profiles of the normalized ion density along the Y (blue) and Z (red) directions in Figure 3b1. The black vertical lines indicates the location of the solar wind shadow boundary and the blue and red vertical lines show the location of the fast mode wave fronts in the Y and Z directions, respectively. (c1, c2, d1, and d2) Same formats as Figures 3b1 and 3b2, but they show data in region II and III, respectively.

compressions are also seen in our data; however, they have been smoothed out by the statistic approach in Figure 4d.

[17] In addition, the fast mode waves may not the only mode existing in the wake system, and the other modes, that is to say, the Alfvén and slow mode waves may also be excited [*Wiehle et al.*, 2011]. In our data, for example, in the solar wind shadow region, the thermal pressure decreases (Figure 4c) and the magnetic pressure (field magnitude) increases compared to the background (Figure 4d). These anti-correlated variations indicate a slow mode perturbation. In this paper, however, our purpose is to identify the WB, so the slow mode boundaries are not determined. In the simulation of *Wiehle et al.* [2011] and *Holmstrom et al.* [2012], there is a region inside the wake with ion number density of the solar wind level. *Wiehle et al.* [2011] noticed that in this region the field perturbations are mainly field-perpendicular,

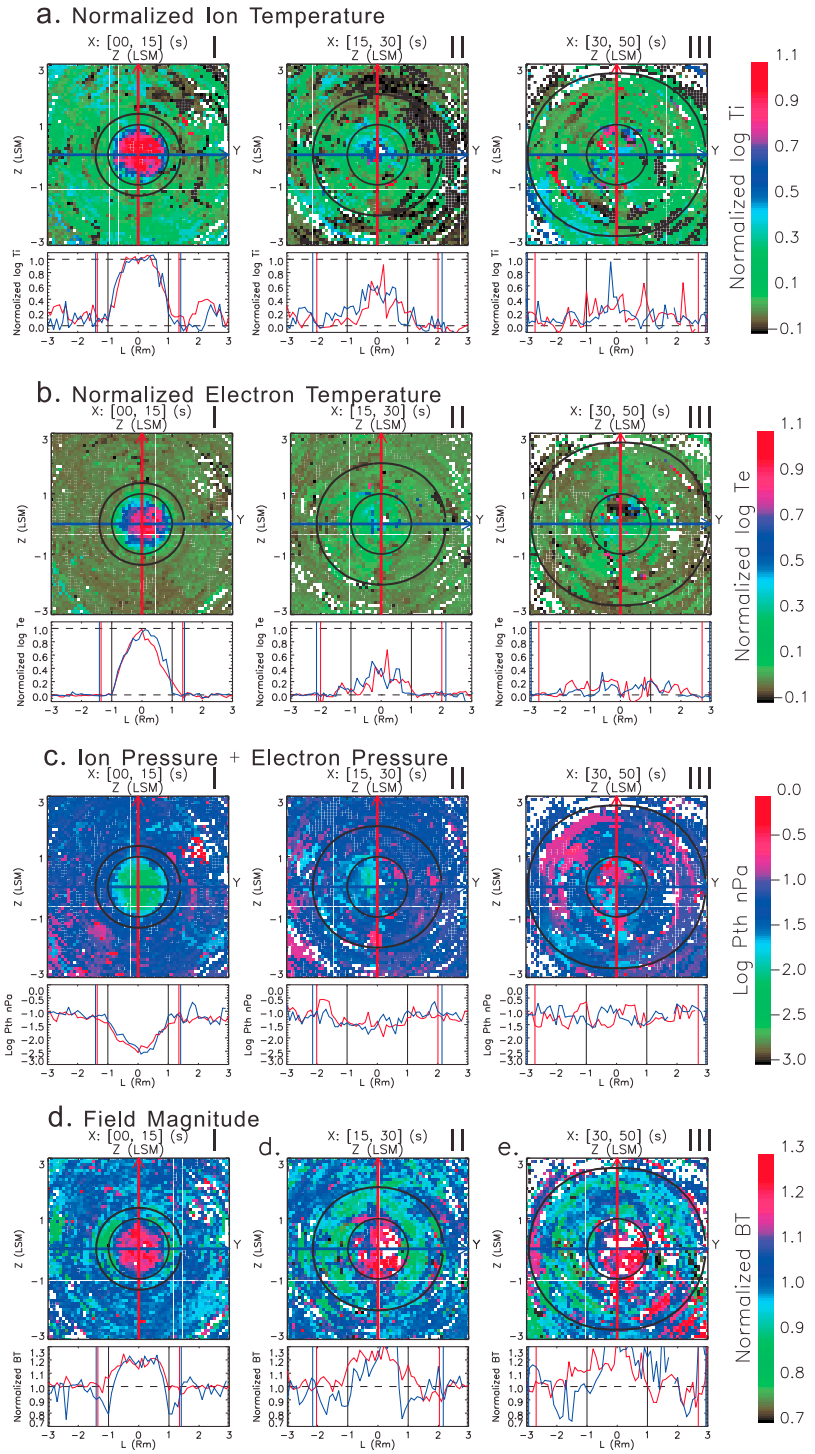

Figure 4. The distributions of the normalized (a) ion temperatures ($T_{i,wake}/T_{i,back}$), (b) electron temperature ($T_{e,wake}/T_{e,back}$), (c) thermal pressure (sum of ion and electron pressures) and (d) field magnitude ($B_{T,wake}/B_{T,Solarwind}$) inside and around the lunar wake. The format of each plot is the same as those in Figure 3.

and they proposed that this perturbation is Alfvénic. However, in our data, this high number density region is not clearly seen.

[18] It should be noticed that the wake discussed in this paper only characterizes the interaction between the supersonic magnetized plasma (solar wind) and non-conductive bodies. To those conductive bodies, such as Io, the moon of the Jupiter, the interaction with the flowing plasma is different. The dense plasma in the ionosphere and torus of Io may slow down the surrounding flowing plasma near the Io and bend the field line to form global Alfvén wings [e.g., *Frank et al.*, 1996].

[19] **Acknowledgments.** This work was supported by the specialized research fund for Chinese state key laboratories under project number Y22612A33S, the KIP Pilot Project (kzcx2-yw-123) of CAS, the National Science Foundation of China (40974090 and 40636032) and National Important Basic Research Project (2006CB806306 and 2011CB811405). Work at UCLA was supported by NASA through THEMIS 443869-TM-22620 and THEMIS/ARTEMIS project NAS5-02099. We also specially acknowledge with appreciation J. McFadden for use of ESA and K. H. Glassmeier, U. Auster and W. Baumjohann for the use of FGM data provided under the lead of the Technical University of Braunschweig and with financial support through the German Ministry for Economy and Technology and the German Center for Aviation and Space (DLR) under contract 50 OC 0302.

[20] The Editor thanks two anonymous reviewers for assisting in the evaluation of this paper.

References

Angelopoulos, V. (2011), The ARTEMIS mission, *Space Sci. Rev.*, *165*, 3–25, doi:10.1007/s11214-010-9687-2.

Auster, H. U., et al. (2008), The THEMIS fluxgate magnetometer, *Space Sci. Rev.*, *141*, 235–264, doi:10.1007/s11214-008-9365-9.

Clack, D., J. C. Kasper, A. J. Lazarus, J. T. Steinberg, and W. M. Farrell (2004), Wind observations of extreme ion temperature anisotropies in the lunar wake, *Geophys. Res. Lett.*, *31*, L06812, doi:10.1029/2003GL018298.

Colburn, D. S., R. G. Currie, J. D. Mihalov, and C. P. Sonett (1967), Diamagnetic solar-wind cavity discovered behind moon, *Science*, *158*, 1040–1042, doi:10.1126/science.158.3804.1040.

Denavit, J. (1979), Collisionless plasma expansion into a vacuum, *Phys. Fluids*, *22*, 1384–1392, doi:10.1063/1.862751.

Farrell, W. M., M. L. Kaiser, J. T. Steinberg, and S. D. Bale (1998), A simple simulation of a plasma void: Applications to Wind observations of the lunar wake, *J. Geophys. Res.*, *103*(A10), 23,653–23,660, doi:10.1029/97JA03717.

Frank, L. A., et al. (1996), Plasma observations at Io with the Galileo spacecraft, *Science*, *274*(5286), 394–395, doi:10.1126/science.274.5286.394.

Halekas, J. S., D. A. Brain, D. L. Mitchell, R. P. Lin, and L. Harrison (2006), On the occurrence of magnetic enhancements caused by solar wind interaction with lunar crustal fields, *Geophys. Res. Lett.*, *33*, L08106, doi:10.1029/2006GL025931.

Halekas, J. S., Y. Saito, G. T. Delory, and W. M. Farrell (2011), New views of the lunar plasma environment, *Planet. Space Sci.*, *59*, 1681–1694, doi:10.1016/j.pss.2010.08.011.

Holmstrom, M., S. Fatemi, Y. Futaana, and H. Nilsson (2012), The interaction between the Moon and the solar wind, *Earth Planets Space*, *64*, 237–245, doi:10.5047/eps.2011.06.040.

Johnson, F. S., and J. E. Midgley (1968), Notes on the lunar magnetosphere, *J. Geophys. Res.*, *73*, 1523–1532, doi:10.1029/JA073i005p01523.

McFadden, J. P., et al. (2008), The THEMIS ESA plasma instrument and in-flight calibration, *Space Sci. Rev.*, *141*, 277–302, doi:10.1007/s11214-008-9440-2.

Michel, F. C. (1968), Magnetic field structure behind the Moon, *J. Geophys. Res.*, *73*, 1533–1542, doi:10.1029/JA073i005p01533.

Ness, N. F., K. W. Behannon, C. S. Searce, and S. C. Cantarano (1967), Early results from the magnetic field instrument on lunar Explorer 35, *J. Geophys. Res.*, *72*, 5769–5778, doi:10.1029/JZ072i023p05769.

Ogilvie, K. W., J. T. Steinberg, R. J. Fitzenreiter, C. J. Owen, A. J. Lazarus, W. M. Farrell, and R. B. Torbert (1996), Observations of the lunar plasma wake from the WIND spacecraft on December 27, 1994, *Geophys. Res. Lett.*, *23*(10), 1255–1258, doi:10.1029/96GL01069.

Omidi, N., X. Blanco-Cano, C. T. Russell, H. Karimabadi, and M. Acuna (2002), Hybrid simulations of solar wind interaction with magnetized asteroids: General characteristics, *J. Geophys. Res.*, *107*(A12), 1487, doi:10.1029/2002JA009441.

Owen, C. J., R. P. Lepping, K. W. Ogilvie, J. A. Slavin, W. M. Farrell, and J. B. Byrnes (1996), The lunar wake at 6.8 RL: Wind magnetic field observations, *Geophys. Res. Lett.*, *23*(10), 1263–1266, doi:10.1029/96GL01354.

Samir, U., K. H. Wright, and N. H. Stone (1983), The expansion of a plasma into a vacuum: Basic phenomena and processes and applications to space plasma physics, *Rev. Geophys.*, *21*(7), 1631–1646, doi:10.1029/RG021i007p01631.

Sibeck, D. G., et al. (2011), ARTEMIS science objectives, *Space Sci. Rev.*, *165*, 59–91, doi:10.1007/s11214-011-9777-9.

Sonett, C. P. (1982), Electromagnetic induction in the Moon, *Rev. Geophys.*, *20*, 411–455, doi:10.1029/RG020i003p00411.

Wang, Y.-C., J. Muller, W.-H. Ip, and U. Motschmann (2011), A 3D hybrid simulation study of the electromagnetic field distributions in the lunar wake, *Icarus*, *216*(2), 415–425, doi:10.1016/j.icarus.2011.09.021.

Whang, Y. C. (1968), Interaction of a magnetized solar wind with the Moon, *Phys. Fluids*, *11*, 969, doi:10.1063/1.1692068.

Whang, Y. C., and N. F. Ness (1970), Observations and interpretation of the Lunar Mach Cone, *J. Geophys. Res.*, *75*, 6002, doi:10.1029/JA075i031p06002.

Wiehle, S., et al. (2011), First lunar wake passage of ARTEMIS: Discrimination of wake effects and solar wind fluctuations by 3D hybrid simulations, *Planet. Space Sci.*, *59*, 661–671, doi:10.1016/j.pss.2011.01.012.